Scientific Reports
https://doi.org/10.1038/s41598-026-39850-4

Article in Press

Model predictive control with adaptive Kalman filter for premixed turbocharged natural gas engine

Received: 26 October 2025
Accepted: 9 February 2026
Published online: 14 February 2026

Cite this article as: Xiong W., Gong Q., Huang S. *et al.* Model predictive control with adaptive Kalman filter for premixed turbocharged natural gas engine. *Sci Rep* (2026). https://doi.org/10.1038/s41598-026-39850-4

Wenyu Xiong, Qichangyi Gong, Songtao Huang, Jie Ye & Jinbang Xu

Model Predictive Control with Adaptive Kalman Filter for Premixed Turbocharged Natural Gas Engine

Wenyu Xiong[1], Qichangyi Gong[2,3,*], Songtao Huang[2,+], Jie Ye[2,+], and Jinbang Xu[2,+]

[1]School of Intelligent Manufacturing, Jianghan University, Wuhan, 470056, China
[2]School of Artificial Intelligence and Automation, Huazhong University of Science and Technology, Wuhan, 470074, China
[3]United Automotive Electronic System Company Limited, Shanghai, 201206, China
[*]qichangyi.gong@uaes.com
[+]these authors contributed equally to this work

ABSTRACT

Robust control of natural-gas engines under unknown load disturbances remains challenging due to strong couplings and delays in multi-input multi-output (MIMO) dynamics. This paper presents a control framework that integrates rate-based model predictive control (MPC) with a gain-scheduling scheme driven by an adaptive Kalman filter to enhance performance under unknown load disturbances. A novel adaptation mechanism enables the Kalman filter to rapidly track transient changes in load torque while attenuating steady-state estimation noise. The online torque estimate is used to compute local equilibrium operating points and generate a gain-scheduling parameter matrix that adaptively adjusts MPC behavior to improve transient response. Experimental validation on a laboratory engine demonstrates that the estimator converges quickly during load transients and maintains low steady-state noise; when combined with gain-scheduled MPC, the proposed controller significantly reduces speed and air-fuel-ratio deviations and shortens settling time following step load changes. The results indicate improved disturbance rejection and practical applicability for power-generation engines.

Introduction

Due to increasingly stringent emission regulations, natural-gas engines–featuring lower carbon intensity and reduced pollutant emissions–are becoming attractive alternatives to conventional gasoline and diesel engines in industrial and power-generation applications[1–3]. This paper focuses on natural-gas engines coupled to synchronous generators for power generation, where engine speed directly determines the generated frequency and voltage. When used as distributed or stand-alone generation units, these engines must reject unknown load disturbances so as to maintain the target speed and to minimize speed deviation and recovery time; concurrently, the air-fuel ratio (AFR) must be kept close to its reference throughout operation to satisfy emission limits. Good disturbance-rejection capability therefore shortens the time to restore frequency and voltage to acceptable levels and ensures reliable power supply. This work seeks a practical control solution that meets these requirements.

Heavy-duty natural-gas engines employed in generator sets typically have many cylinders and large displacement. Compared with electronic fuel-injection (EFI) strategies[4], premixed intake (pre-mixer) configurations[5] are often preferred in such engines for lower cost and more uniform mixture formation; however, premixing introduces strong actuator-output couplings, producing a challenging multi-input multi-output (MIMO) control problem[6].MPC is a promising approach for such strongly coupled MIMO systems because it coordinates multiple actuators through an explicit cost function. Prior work has applied MPC to various engine subsystems, including boost-pressure and exhaust gas recirculation (EGR) control for two-stage turbocharged engines[7], nonlinear MPC for turbocharged SI engines with dual-loop EGR[8], heavy-duty diesel control[9], and engine-speed regulation[10,11], demonstrating MPC's advantages in handling multivariable interactions. Engine dynamics are inherently nonlinear. While nonlinear MPC is conceptually attractive, practical deployment is challenged by the computational complexity of solving nonlinear optimal control problems on embedded hardware, which limits achievable prediction horizons[6,12]. A common alternative linearizes the nonlinear model at an operating point and employs linear parameter-varying or gain-scheduling MPC (LPV-MPC)[13,14]. To guarantee zero steady-state error under disturbances, linear MPC variants have used integral state augmentation[11], disturbance estimators that compensate model-plant mismatch[15], or rate-based MPC formulations[16]. However, integrator augmentation risks windup and complicates constraint handling in MIMO settings; disturbance-state augmentation increases model order and implementation complexity. Rate-based MPC offers a practical compromise, but for the large and rapidly varying load disturbances considered here, rate-based MPC alone does not deliver the required transient performance. To address this, we combine rate-based MPC with a simple independent load estimator and a gain-scheduling strategy.

The load estimator is intentionally kept simple and aims solely to observe the external load torque; its output, together with the tracking references, drives the gain-scheduling mechanism. In practice, however, simple observers are sensitive to measurement noise and can inject irregular perturbations into throttle commands, degrading tracking performance. Thus a Kalman filter is introduced. While the extended Kalman filter (EKF) is commonly used[17], its reliance on local linearization can incur significant linearization error and poor robustness to model uncertainty. The unscented Kalman filter (UKF) improves linearization accuracy via the unscented transform[18] but incurs high computational cost that limits its applicability on embedded platforms. Hybrid Kalman filters (HKF)[19,20], which retain key nonlinear terms, strike a balance by reducing linearization error with modest complexity. Motivated by HKF, this paper develops a compact second-order linear Kalman filter tailored for load-torque estimation and decoupled from the original fourth-order engine model.

A fundamental trade-off for Kalman filters exists between noise suppression and tracking agility: filters tuned for strong noise rejection tend to track slowly. To overcome this, prior works have used adaptive tuning and strong-tracking modifications that adapt the estimator covariance according to an adaptive law[21–23]. Building on these ideas, we propose a load-detection-based adaptive strategy that rapidly increases estimator responsiveness during transients while preserving noise attenuation in steady state. The resulting adaptive Kalman filter provides fast, robust load-torque estimates that are suitable for online use in gain scheduling. The main contributions of this paper are:

(1) A novel adaptive Kalman filter is presented with a mechanism for rapid tracking of transient load changes and attenuation of steady-state noise.

(2) A hybrid control framework is developed that integrates predictive control of the rate-based model with a gain scheduling strategy driven by an adaptive Kalman filter, allowing enhanced rejection of unknown load disturbances in natural-gas generator sets.

(3) Experimental implementation and validation are presented, demonstrating that the proposed adaptive MPC scheme effectively reduces engine speed and AFR fluctuations and shortens settling time under varying load conditions, confirming its superior transient performance and suitability for embedded implementation.

Engine Model

Engine Physical Model

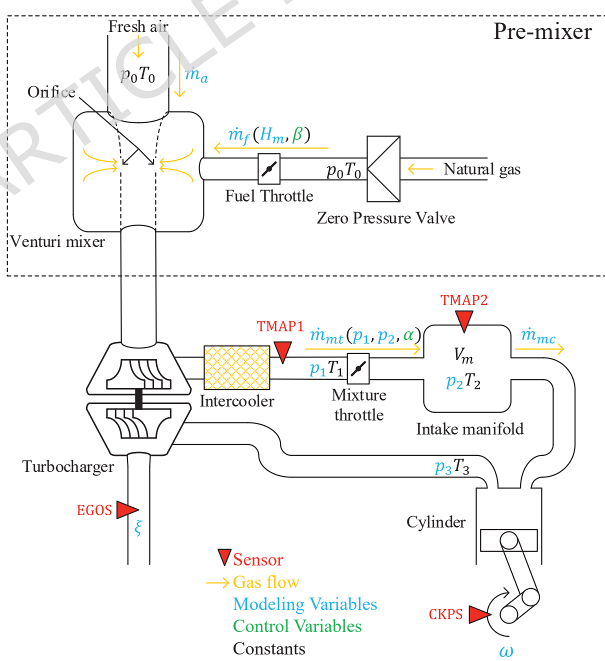

Figure 1. Pre-mixed turbocharged CNG engine.

The structure of this engine is schematically shown in Figure 1. The air path consists of two main sections: the pre-mixer and the turbocharged engine section. The pre-mixer primarily includes a Venturi mixer and a fuel throttle. A zero-pressure valve is installed upstream of the fuel throttle to maintain inlet pressure at atmospheric level. Natural gas is drawn into the Venturi mixer through orifices via the Venturi effect, with the fuel throttle opening β regulating the natural gas mass flow rate. The second section resembles a conventional turbocharged engine, where the mixture throttle opening α controls the mass flow of the mixed gas. Two temperature and manifold absolute pressure sensors (TMAP1 and TMAP2) are employed to monitor the temperature and pressure of the boosted mixture downstream of the compressor and the gas in the intake manifold, respectively. A crankshaft position sensor (CKPS) measures the crankshaft phase and rotational speed. An exhaust gas oxygen sensor (EGOS) is mounted on the exhaust pipe to determine the AFR.

The engine model employed in this study is adopted from the authors' prior work[6] and is presented below:

$$\begin{cases} \dot{\omega} = \dfrac{1}{J}\left[\tau_e - k_b\omega - \tau_p - \tau_L\right] \\ \dot{\xi} = H_m \dfrac{\dot{m}_f}{\dot{m}_a}\dfrac{1}{\xi+1} - \dfrac{\xi}{\xi+1} \\ \dot{p}_2 = \dfrac{R_m T_2}{V_m}\left(\dot{m}_{mt} - \dot{m}_{mc}\right) \\ \dot{p}_1 = \dfrac{R_m T_1}{V_t}\left(\dot{m}_c - \dot{m}_{mt}\right) \end{cases} \tag{1}$$

where

$$\tau_e = \eta_e \frac{\xi(t-t_d)}{\xi(t-t_d)+1}\dot{m}_{mc} \tag{2}$$

$$t_d = \frac{p_1 V_T}{R_m T_1}\cdot\frac{1}{\dot{m}_{mc}} = \frac{p_1 V_T T_2}{\omega V_d \eta_{ch} p_2 T_1} \tag{3}$$

$$\dot{m}_{mc} = \frac{\omega V_d \eta_{ch} p_2}{4\pi R_m T_2} \tag{4}$$

$$H_m \frac{\dot{m}_f}{\dot{m}_a} = H_m \frac{C_f S_{thvm}}{C_a S_a}\sqrt{\frac{R_a}{R_f}}\left[1 - \cos\left(\frac{\beta\pi}{180}\right)\right] \tag{5}$$

$$\dot{m}_{mt} = C_m S_m \left[1 - \cos\left(\frac{\alpha\pi}{180}\right)\right]\frac{p_1}{\sqrt{R_m T_1}}\Psi\left(\frac{p_2}{p_1}\right) \tag{6}$$

$$\Psi\left(\frac{p_2}{p_1}\right) = \begin{cases} \kappa^{\frac{1}{2}}\left(\frac{2}{\kappa+1}\right)^{\frac{\kappa+1}{2(\kappa-1)}} & \frac{p_2}{p_1} \le \kappa_c \\ \sqrt{\frac{2\kappa}{\kappa-1}\left[\left(\frac{p_2}{p_1}\right)^{\frac{2}{\kappa}} - \left(\frac{p_2}{p_1}\right)^{\frac{\kappa+1}{\kappa}}\right]} & \frac{p_2}{p_1} > \kappa_c \end{cases} \tag{7}$$

$$H_m = \begin{cases} a_1\dot{m}_{mt}^2 + a_2\dot{m}_{mt} + a_3 & \dot{m}_{mt} \le m_{hc} \\ 1 & \dot{m}_{mt} > m_{hc} \end{cases} \tag{8}$$

This is a fourth-order nonlinear model with state variables of engine speed ω(rad/s), the fuel-air ratio ξ in the Venturi mixer, intake manifold pressure p_2(Pa), and boost pressure p_1(Pa). The state variable is chosen as the fuel-air ratio ξ rather than the AFR to avoid the fuel throttle opening β appearing in the denominator, which would introduce additional nonlinearities into the model dynamics. The first equation in Eq.1 describes the crankshaft rotation dynamics. Here, J is the rotational inertia, k_b is the friction coefficient, τ_p is the mechanical and pumping loss torque, and τ_L is the unknown load torque disturbance. The indicated torque τ_e is defined by Eq.2, where η_e is the engine efficiency coefficient (obtained from look-up tables as a function of speed, AFR, and ignition angle). A significant AFR transport delay t_d, given by Eq.3, is incorporated into τ_e because the mixture ratio takes time to reach the cylinders. In Eq.3, V_T is the pipe volume from the mixer to the cylinders, T_1 is the boost temperature, and R_m is the gas constant of the mixed gas. The mass flow rate of the mixture into the cylinders $\dot{m}_{mc}$, is given by Eq.4, where V_d is the engine displacement, T_2 is the intake manifold temperature, and η_{ch} is the volumetric efficiency (obtained from look-up tables).

The second equation in Eq.1 governs the natural gas and air mixing dynamics within the Venturi mixer. The term $H_m \frac{\dot{m}_f}{\dot{m}_a}$ is defined by Eq.5. Here, H_m is an empirical correction factor. Its primary role is to compensate for the deviation between the theoretical fuel-air flow ratio $\frac{\dot{m}_f}{\dot{m}_a}$ and the actual value, which arises from model simplifications, sensor inaccuracies, and actual flow characteristics. Introducing this coefficient can significantly improve the model's predictive accuracy regarding the actual system behavior. The value of H_m is a function of the mixture throttle mass flow rate $\dot{m}_{mt}$. It is determined by identifying parameters from experimental data, and its specific expression is given by the piecewise function shown in Eq.8.

The third and fourth equations in Eq.1 describe the gas filling dynamics for the intake manifold pressure and boost pressure, respectively. The mass flow rate through the mixture throttle, $\dot{m}_{mt}$, is given by Eq.6, where C_m and S_m are constants, and the flow function $\Psi(p_2/p_1)$ defined by Eq.7. The compressor mass flow rate is denoted by $\dot{m}_c$.

As evident from the equations, this fourth-order model represents a dual-input, dual-output system. The control inputs are the mixture throttle opening α and the fuel throttle opening β, and the outputs are engine speed ω and fuel-air ratio ξ. All four state variables are measurable. A key characteristic is the strong coupling between inputs and outputs, as both ω and ξ are simultaneously influenced by α and β.

Model Linearization and Discretization

The nonlinear engine model is linearized around various equilibrium points to facilitate controller design. Defining the state vector $x = [\omega \quad \xi \quad p_2 \quad p_1]^T$, control inputs as $u = [\alpha \quad \beta]^T$, disturbance as $d = \tau_L$, and outputs as $y = [\omega \quad \xi]^T$, the nonlinear system described by Eq.1 can be expressed in compact form as:

$$\dot{x} = f(x, u, d) \tag{9}$$

Consider an equilibrium point defined by $x_{ss} = [\omega_{ss} \quad \xi_{ss} \quad p_{2_{ss}} \quad p_{1_{ss}}]^T$ and steady-state inputs $u_{ss} = [\alpha_{ss} \quad \beta_{ss}]^T$, which satisfy the equilibrium condition $0 = f(x_{ss}, u_{ss}, 0)$. By introducing deviation variables $\delta x = x - x_{ss}$, $\delta u = u - u_{ss}$, and applying first-order Taylor series expansion, the system is linearized to obtain the linear time-invariant representation:

$$\begin{aligned} \delta\dot{x} &= A_c \delta x + B_{1c} \delta u + B_{2c} d \\ \delta y &= C_c \delta x \end{aligned} \tag{10}$$

where A_c, B_{1c} and B_{2c} represent the Jacobian matrices of f with respect to x_{ss}, u_{ss} and d, respectively, evaluated at the equilibrium point $(x_{ss}, u_{ss}, 0)$.

The continuous-time linear model in Eq.10 is then discretized using a sampling period of $t_{s1} = 50$ms, yielding the discrete-time state-space representation:

$$\begin{aligned} \delta x(k+1) &= A_d \delta x(k) + B_{1d} \delta u(k) + B_{2d} d(k) \\ \delta y(k) &= C_d \delta x(k) \end{aligned} \tag{11}$$

where the discrete-time matrices are computed as:

$$A_d = e^{A_c t_{s1}}; B_{id} = \left(\int_0^{t_{s1}} e^{A_c t_{s1}} \, \mathrm{d}t \right) B_{ic}, (i = 1, 2); C_d = C_c$$

Time Delay Prediction

In the engine model described by Eq.1, the second equation characterizes the mixing dynamics at the Venturi mixer. However, the mixed gas must traverse the turbocharger, intercooler, and intake manifold before reaching the cylinders: a process that introduces a significant transport delay. This delay, denoted t_d, must be accounted for in the fuel-air ratio variable ξ. As given by Eq.3, t_d varies with engine operating conditions, specifically speed ω and intake manifold pressure p_2. Let $t_d = n_d t_{s1}$, where $t_{s1} = 50$ms is the sampling period. The fuel-air ratio measured at the Venturi mixer only be observed at the EGOS after n_d sampling intervals. To predict the current state affected by this delay, past state variables are utilized. Define a delayed state vector $\delta x'(k - n_d) = [\delta\omega(k - n_d) \quad \delta\xi(k) \quad \delta p_2(k - n_d) \quad \delta p_1(k - n_d)]^T$, where $\xi(k)$ is the fuel-air ratio measured at the EGOS at time k, which corresponds to the ratio at the Venturi mixer at time $k - n_d$. Using the discrete-time model Eq.11, the current state can be iteratively predicted as:

$$\delta x'(k) = {A_d}^{n_d} \delta x'(k - n_d) + \sum_{i=1}^{n_d} {A_d}^{n_d - i} B_{1d} \delta u(k - (n_d - i + 1)) + \sum_{i=1}^{n_d} {A_d}^{n_d - i} B_{2d} d(k - (n_d - i + 1)) \tag{12}$$

The second element of $\delta x'(k)$, denoted $\delta\xi'(k)$, represents the predicted fuel-air ratio at the Venturi mixer at the current time k. By replacing all instances of $\xi(t - t_d)$ in Eq.1 with $\xi'(k)$, a new state vector $x_p(k) = [\delta\omega(k) \quad \delta\xi'(k) \quad \delta p_2(k) \quad \delta p_1(k)]^T$ is obtained, which is used for subsequent controller design.

A common alternative for handling delays in MPC is to incorporate the delay directly into the model, forming an augmented system[11]. However, this approach increases model dimension proportionally to the number of delay steps. Given the large and variable delay in our application, the augmentation method becomes impractical. Instead, the proposed prediction-based iteration offers a more efficient solution, wherein variations in t_d only affect the number of prediction steps n_d, without altering the controller structure.

MPC Controller Design

Linear MPC Design

The reference signal is defined as $r(k) = [\omega_r(k) \quad \xi_r(k)]^T$, which is treated as constant over the prediction horizon. Conventional MPC for reference tracking typically minimizes a quadratic cost function based on the difference between predicted outputs and target values. While this approach using Eq.11 can theoretically achieve zero steady-state error when there is perfect model-plant match, such ideal conditions are rarely attainable in practice. To address this limitation, this paper employs a rate-based MPC formulation with a difference-scheme augmented model. Define the incremental variables: $\Delta x_p(k) = \delta x_p(k) - \delta x_p(k-1)$, $\Delta u(k) = \delta u(k) - \delta u(k-1)$, $\Delta d(k) = d(k) - d(k-1)$, and $\Delta y(k) = \delta y(k) - \delta y(k-1)$. The discrete-time model from Eq.11 can be reformulated as:

$$\begin{aligned} \Delta x_p(k+1) &= A_d \Delta x_p(k) + B_{1d}\Delta u(k) + B_{2d}\Delta d(k) \\ \Delta y(k) &= C_d \Delta x(k) \end{aligned} \tag{13}$$

A new state vector is constructed as $x_m(k) = [\Delta x_p(k)^T \quad \delta y(k)^T]^T$, yielding the augmented state-space model:

$$\begin{aligned} \underbrace{\begin{bmatrix} \Delta x_p(k+1) \\ \delta y(k+1) \end{bmatrix}}_{x_m(k+1)} &= \underbrace{\begin{bmatrix} A_d & 0 \\ C_d A_d & I \end{bmatrix}}_{A} \underbrace{\begin{bmatrix} \Delta x_p(k) \\ \delta y(k) \end{bmatrix}}_{x_m(k)} + \underbrace{\begin{bmatrix} B_{1d} \\ C_d B_{1d} \end{bmatrix}}_{B_1} \Delta u(k) + \underbrace{\begin{bmatrix} B_{2d} \\ C_d B_{2d} \end{bmatrix}}_{B_2} \Delta d(k) \\ \underbrace{\begin{bmatrix} \delta y(k) \end{bmatrix}}_{y_m(k)} &= \underbrace{\begin{bmatrix} 0 & I \end{bmatrix}}_{C} \underbrace{\begin{bmatrix} \Delta x_p(k) \\ \delta y(k) \end{bmatrix}}_{x_m(k)} \end{aligned} \tag{14}$$

This augmented formulation offers two significant advantages. First, by selecting the equilibrium point to coincide with the reference signal (i.e., $y_{ss} = r(k)$), the control objective simplifies to driving the output of Eq.14 to zero at steady state. This eliminates the need for explicit reference tracking terms in the cost function. Second, the incremental state formulation inherently ensures zero steady-state tracking error without requiring additional integrator states[24].

The prediction model is constructed as follows. Since the disturbance $d(k)$ is unknown and assumed constant over the prediction horizon, the term $B_2\Delta d(k)$ is omitted from predictions:

$$Y = F x_m(k) + \Phi \Delta U \tag{15}$$

where

$$\begin{aligned} Y &= [y_m(k+1|k)^T \quad y_m(k+2|k)^T \cdots y_m(k+H_p|k)^T]^T \\ \Delta U &= [\Delta u(k)^T \quad \Delta u(k+1)^T \cdots \Delta u(k+H_c-1)^T]^T \\ F &= [(CA)^T \quad (CA^2)^T \cdots (CA^{H_p})^T]^T \\ \Phi &= \begin{bmatrix} CB_1 & 0 & \cdots & 0 \\ CAB_1 & CB_1 & \cdots & 0 \\ \vdots & & & \\ CA^{H_p-1}B_1 & CA^{H_p-2}B_1 & \cdots & CA^{H_p-H_c}B_1 \end{bmatrix} \end{aligned}$$

Here, H_p and H_c denote the prediction and control horizons, respectively. The cost function weights the output and control increments:

$$min \quad J = Y^T Q Y + \Delta U^T R \Delta U \tag{16}$$

where Q and R diagonal weighting matrices. The optimization variable ΔU contains the sequence of control increments, with the actual control input computed as:

$$u(k) = u_{ss} + \delta u(k) = u_{ss} + \sum_{i=0}^{k} \Delta u(i) \tag{17}$$

where $\Delta u(k)$ represents the first element of the optimal ΔU sequence. Practical constraints are implemented as follows. Rate constraints prevent excessive throttle movements that could destabilize the Venturi mixer flow or cause turbocharger surge:

$$\begin{aligned} \Delta u_{min} \leq &\Delta u(k) \leq \Delta u_{max} \\ u_{min} - u(k-1) \leq &\Delta u(k) \leq u_{max} - u(k-1) \end{aligned} \tag{18}$$

These constraints apply to all elements in the ΔU sequence over the control horizon.

Optimization Problem Solution

The optimization problem defined by Eq.16 is commonly solved by converting it into a standard quadratic programming (QP) formulation, for which efficient and numerically reliable solvers are available. Substituting the prediction model from Eq.15 into the cost function, and treating the state vector $x_m(k)$ as known over the prediction horizon at each control instant, the constrained optimization problem can be rewritten as:

$$\min_{\Delta U} J_{QP} = \frac{1}{2}[\Delta U^T(2\Phi^T Q\Phi + 2R)\Delta U] + 2\Delta U^T \Phi^T QFx_m(k) + x_m^T(k)F^T QFx_m(k) s.t. \quad Z\Delta U \leq W \tag{19}$$

This constitutes a typical QP problem. The constraint matrices Z and W are readily constructed from the rate and amplitude limits given in Eq.18. Since the weighting matrices Q and R are diagonal with positive entries, the Hessian matrix $2(\Phi^T Q\Phi + R)$ is symmetric positive definite. Therefore, the optimization problem in Eq.19 is strictly convex and can be solved efficiently online using active-set methods[25]. The solution yields the optimal sequence ΔU, from which only the first element $\Delta u(k)$ is applied to the plant via Eq.17; the remaining elements are discarded in accordance with the receding horizon principle.

A key observation is that the QP formulation depends solely on $x_m(k)$, F, and Φ. Since $x_m(k)$ is measurable or computable online, and both F and Φ are functions only of the linearized engine model at a given equilibrium point, these matrices can be precomputed offline for a set of operating conditions and stored in look-up tables. As a result, the online computational burden of the MPC reduces essentially to solving a QP problem at each sampling instant, making the strategy suitable for embedded implementation.

Adaptive Kalman Filter and Gain Scheduling Strategy

While the previous section completed the design of an MPC controller for a single equilibrium point, and prior work[16] has demonstrated that rate-based MPC can compensate for certain model-plant mismatches, treating the load torque purely as a model mismatch reveals limitations. Although the controller can eventually regulate the system back to the target operating point, its inherent compensation capability is insufficient to meet the stringent requirements for speed and AFR fluctuation ranges in power generation applications. Therefore, an alternative method to enhance load response performance is necessary.

A conventional approach involves treating the load torque as an additional state variable, constructing a fifth-order state-space model and observer. However, this method significantly increases model complexity. Re-examining the control design context, the natural gas engine studied herein operates primarily at a single nominal working point: 1500 rpm engine speed with a stoichiometric AFR. Although this suggests a single equilibrium point, the engine's internal state actually shifts under load variations. While the controlled outputs ω and ξ return to their references in steady state following a load change, the pressures p_2 and p_1 settle at new values. This indicates that the equilibrium point itself moves with the load.

Consequently, the linearized model corresponding to the new operating point must be updated, and the MPC controller should be adjusted accordingly, affecting the incremental control signals Δu and δu. Furthermore, referring to Eq.17, the shift in the equilibrium point also changes the steady-state input u_{ss}. This implies that during each control interval, in addition to the corrective action $\delta u(k)$ computed by the MPC, an additional feedforward compensation Δu_{ss} can be applied based on the updated equilibrium point. This adjustment, which actively accounts for the changing operating condition, is referred to as the gain scheduling strategy in this paper. The subsequent challenge, therefore, is to accurately estimate the load torque in order to detect and respond to these equilibrium point movements.

Simple Form of Load Estimator Based on Kalman Filter

In practical applications, engine systems are inevitably subject to measurement noise, which can degrade throttle control accuracy, induce throttle jitter, and reduce actuator longevity. To address this issue, a Kalman filter is employed as a load torque estimator.

Reexamining the original engine model in Eq.1, the load torque τ_L appears only in the speed dynamics. Since all four state variables are measurable and the remaining three differential equations are independent of τ_L, only the speed dynamics equation is utilized for estimator design. By treating τ_L as an additional state variable and incorporating process and measurement noise, a second-order system is formulated as follows:

$$\begin{aligned} \dot{\omega} &= \frac{1}{J}[\tau_e - k_b\omega - \tau_p - \tau_L + \upsilon_t] \\ \dot{\tau}_L &= \upsilon_{tl} \end{aligned} \tag{20}$$

where υ_t and υ_{tl} represent mutually independent, zero-mean Gaussian noise terms associated with the reconstructed engine torque and the load torque derivative, respectively[26]. By defining $u_e = \tau_e - \tau_p$ as an input, the nonlinearities in τ_e are avoided, resulting in a simple second-order linear model. This formulation is physically justified since the net torque (engine output minus load) determines the rotational acceleration.

Discretizing the system with a sampling period t_{s2} yields the discrete-time state-space model:

$$\underbrace{\begin{bmatrix}\omega(k+1)\\ \tau_L(k+1)\end{bmatrix}}_{x_e(k+1)} = \underbrace{\begin{bmatrix}1-\frac{t_{s2}k_b}{J} & -\frac{t_{s2}}{J}\\ 0 & 1\end{bmatrix}}_{A_e}\underbrace{\begin{bmatrix}\omega(k)\\ \tau_L(k)\end{bmatrix}}_{x_e(k)} + \underbrace{\begin{bmatrix}\frac{t_{s2}}{J}\\ 0\end{bmatrix}}_{B_e}\underbrace{(\tau_e(k)-\tau_p)}_{u_e} + \underbrace{\begin{bmatrix}\frac{t_{s2}}{J} & 0\\ 0 & t_{s2}\end{bmatrix}}_{L}\underbrace{\begin{bmatrix}\upsilon_t(k)\\ \upsilon_{tl}(k)\end{bmatrix}}_{\Upsilon(k)}$$
$$y_e(k) = \underbrace{\begin{bmatrix}1 & 0\end{bmatrix}}_{H}\underbrace{\begin{bmatrix}\omega(k)\\ \tau_L(k)\end{bmatrix}}_{x_e(k)} + \varepsilon \tag{21}$$

where ε is the zero-mean speed measurement noise. Since this model is independent of the controller, and this paper has high requirements for the fast tracking ability of the estimator, the control period of this model can be shorter than the controller, and it is set to be $t_{s2} = 10$ms. Then the linear Kalman filter can be given by[27]:

$$\begin{aligned}
\hat{x}_e^-(k) &= A_e\hat{x}_e^+(k-1) + B_e u_e\\
P^-(k) &= A_e P^+(k-1)A_e^T + M\\
K(k) &= P^-(k)H^T(HP^-(k)H^T+N)^{-1}\\
\hat{\varepsilon}(k) &= \omega(k) - H\hat{x}_e^-(k)\\
\hat{x}_e^+(k) &= \hat{x}_e^-(k) + K(k)\varepsilon(k)\\
P^+(k) &= (I-K(k)H)P^-(k)
\end{aligned} \tag{22}$$

where

$K(k)$: Kalman filter gain matrix

$\hat{x}_e^-(k), \hat{x}_e^+(k)$: a priori and a posteriori state vector

$P^-(k), P^+(k)$: a priori and a posteriori state estimation error covariance matrices

M: Covariance matrix of Υ

N: Variance of ε

$\hat{\varepsilon}(k)$: a priori prediction error

Since $u_e = \tau_e - \tau_p$ is readily available at each control instant, and the output matrix H is scalar-valued, the matrix inversion in the gain update reduces to a scalar division. This structure allows for efficient embedded implementation without requiring the full nonlinear engine model.

Adaptation Mechanism of Kalman Filter

When employing a Kalman filter as an estimator, a well-known trade-off exists between its noise suppression capability and fast tracking performance, it is difficult to achieve both optimally simultaneously. However, in the context of this study, the estimator is required to possess a fast convergence speed to promptly detect load variations and trigger equilibrium point switching, while also maintaining excellent noise attenuation in steady state to ensure accurate and stable throttle opening tracking. To address these competing requirements, this paper introduces an adaptive tuning strategy.

In Eq.22, since A_e,B_e and H are constants, the covariance matrix M and the noise variance N become the primary tuning parameters of the Kalman filter. These are defined as:

$$N = [n_\omega] \quad ; \quad M = \begin{bmatrix} m_t & 0\\ 0 & m_{tl}\end{bmatrix}$$

According to references[21,27,28], the parameter N significantly influences the convergence performance, while M affects the convergence rate. In particular, increasing the element m_{tl} in M enhances the response speed of the corresponding state variable τ_L. Thus, the core idea of the adaptation strategy is to increase m_{tl} during load transients to accelerate load torque tracking, and reduce it after convergence to restore steady-state noise suppression.

To detect load changes, the sliding-window average of the a priori prediction error $\hat{\varepsilon}(k)$ is used[29]:

$$\hat{\varepsilon}_{sw}(k) = \frac{1}{n}(\hat{\varepsilon}(k) + \hat{\varepsilon}(k-1) + \cdots + \hat{\varepsilon}(k-n+1)) \tag{23}$$

When $\hat{\varepsilon}(k)$ resembles white noise, $\hat{\varepsilon}_{sw}(k)$ remains close to zero at steady state. A load change causes $\hat{\varepsilon}_{sw}(k)$ to deviate from zero, enabling the detection of loading/unloading events. As illustrated in Figure 2, the absolute value $|\hat{\varepsilon}_{sw}(k)|$ is fed into a hysteresis comparator. When $|\hat{\varepsilon}_{sw}(k)|$ exceeds an upper threshold ε_{up}, the comparator outputs 1, triggering an increase in m_{tl}; when it falls below a lower threshold ε_{low}, he output becomes 0, and m_{tl} is reset to its initial value.

Furthermore, the following specific and feasible parameter tuning methods are provided:

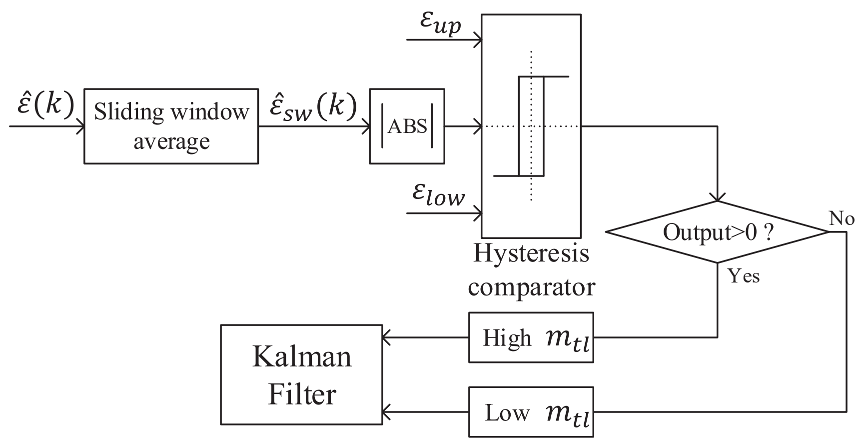

Figure 2. Block diagram of Load change detection adaptation mechanism

- References[30,31] indicate that a sufficient condition for Kalman filter convergence is $N > HP^{+}(k)H^{T}$. However, an excessively large N may reduce the Kalman gain $K(k)$ and slow down convergence. Thus, N is determined as $N = HP^{+}(k)H^{T} + \zeta$, where ζ is appropriately chosen.

- Both m_t and m_{tl} can be set to small values at steady state. Upon detecting a load change, only m_{tl} is increased to ensure fast convergence of the load torque estimate. Once convergence is achieved ($|\hat{\varepsilon}_{sw}(k)| < \varepsilon_{low}$), m_{tl} is reduced back to its initial value.

The effectiveness of this parameter tuning strategy is validated experimentally in the subsequent section.

Gain Scheduling Strategy

The primary objective of gain scheduling is to linearize a nonlinear model at various equilibrium points, thereby generating a family of linear models, each associated with a specific operating condition. A corresponding linear controller is then designed for each equilibrium point. When the operating point shifts, the controller is accordingly switched[32]. In this study, the equilibrium point depends on the load torque, which is considered an unknown disturbance. Thanks to the adaptive Kalman filter proposed in the previous section, an accurate and rapid estimate of the load torque $\hat{\tau}_L$ can be obtained, enabling fast switching of the equilibrium point and completing the basic gain scheduling framework.

However, directly switching the entire controller in practical applications is often overly complex. Since different equilibrium points require distinct controllers, this approach demands substantial data storage and interpolation within lookup tables. To mitigate this, the present work adopts a "low complexity gain scheduling strategy"[33]. This method employs a single linearized model—designed specifically at a nominal equilibrium point—to construct a single MPC. The key idea is to compute a gain variation of the model induced by the equilibrium point shift, which is then used to correct the output of the MPC, making it suitable for the model at the new operating point. Specifically, the nominal equilibrium point is set at 1500rpm engine speed, stoichiometric AFR, and no-load condition. The transfer function linearized at this point is denoted as $P_0(z)$. When the operating point changes, the model at other equilibrium points is represented by $P_\zeta(z)$, where the scheduling parameter ζ corresponds to the estimated load torque. Under nominal conditions, the controller output acts directly on the plant $P_0(z)$. When the equilibrium point shifts, a gain scheduling matrix G_M is introduced such that the corrected plant $G_M P_\zeta(z)$ approximates $P_0(z)$, allowing the same controller to be applied. In this paper, G_M is selected to match the DC gain of the off-nominal model to that of the nominal model:

$$G_M = P_0(1)P_\zeta^{-1}(1) \tag{24}$$

Figure 3(a) and (b) illustrate the control block diagrams under the nominal and off-nominal equilibrium points, respectively. The nominal case is straightforward: the steady-state input u_{ss} is known, and the state $x(k)$ is measurable, leading to a simple controller implementation. In the off-nominal case (Fig. 3(b)), a Kalman filter quickly provides the load torque estimate, enabling the equilibrium point to be updated. Using the nominal model $P_0(z)$, the DC gain is computed to determine G_M. The MPC remains designed based on the nominal linearized model, and its output is corrected via G_M. The incremental control δu

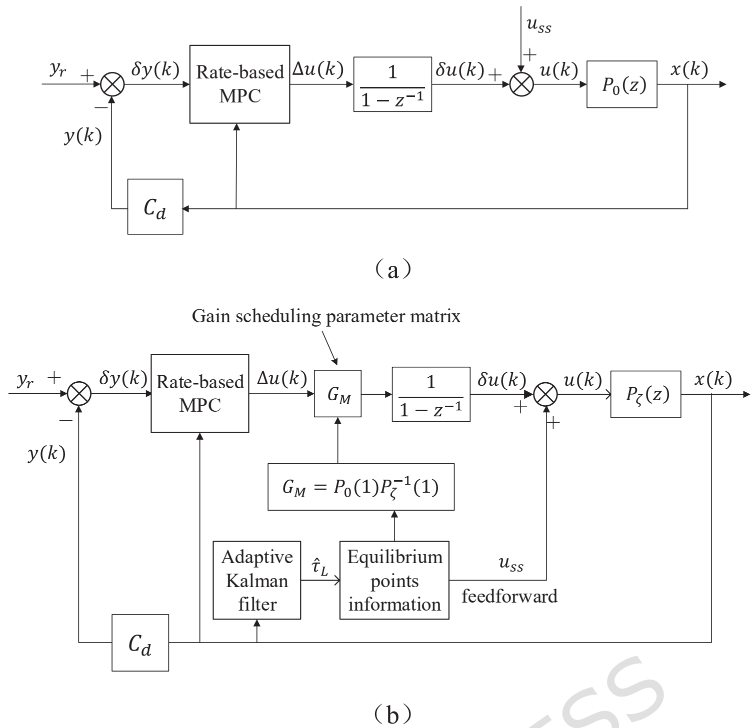

Figure 3. (a) Block diagram under the nominal equilibrium point. (b)Block diagram of gain scheduling under other equilibrium points.

is obtained through integration, and the final control $u(k)$ is formed by adding δu to updated u_{ss}, which acts as a feedforward term. This approach only requires storing the G_M matrix for each load condition, while the controller itself remains unchanged, significantly reducing the need for interpolation and storage. For the dual-input dual-output system considered here, G_M a 2×2 matrix, further alleviating the computational burden.

Experimental Validation

The experimental investigation was performed on a natural gas engine-generator set, as shown in Figure 4. The system comprised an engine directly coupled to a three-phase synchronous generator, which supplied power to a programmable load cabinet for precise load control. The engine had a rated power of 155 kW, a rated speed of 1500rpm, and a maximum torque of 1000Nm. To maintain a stable grid frequency of 50 Hz, the engine speed was controlled at 1500rpm, while the AFR was maintained near the stoichiometric ratio for optimal combustion.

Adaptive Kalman Filter Verification

As previously discussed, the Kalman filter operates independently from the fourth-order nonlinear model and MPC controller, allowing it to utilize a shorter sampling period ($t_{s2} = 10$ms) for enhanced response speed. This study compares three Kalman filter configurations: a low-speed response Kalman filter (L-KF), a high-speed response Kalman filter (H-KF), and the proposed adaptive Kalman filter (A-KF). Both L-KF and H-KF employ fixed parameters, where m_t and m_{tl} remain constant throughout operation. The L-KF utilizes small values for both parameters, while the H-KF employs a significantly larger m_{tl} value (with m_{tl} maintained at the same small value as L-KF) to improve load torque tracking performance. In contrast, the A-KF dynamically adjusts m_{tl} based on the load change detection mechanism: it increases m_{tl} during loading/unloading transients and decreases it once convergence is achieved. The parameter N is identical across all three filters. The sliding window length is carefully selected to balance detection sensitivity and noise immunity—excessively long windows delay load change detection, while overly short windows introduce more white noise into the averaged signal.

The specific parameter configurations for each filter are as follows:

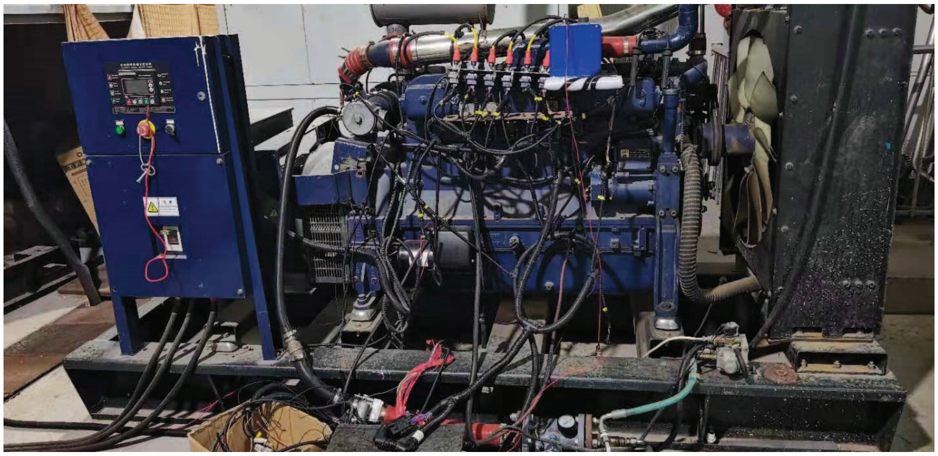

Figure 4. Natural gas engine test bench

- L-KF:

$$N = HP^{+}(k)H^{T} + \zeta \qquad \zeta = 20(rad/s)^2$$
$$m_t = 25(N \cdot m)^2 \qquad m_{tl} = 100(N \cdot m)^2$$

- H-KF:

$$N = HP^{+}(k)H^{T} + \zeta \qquad \zeta = 20(rad/s)^2$$
$$m_t = 25(N \cdot m)^2 \qquad m_{tl} = 5 \times 10^4 (N \cdot m)^2$$

- A-KF:

$$N = HP^{+}(k)H^{T} + \zeta \qquad \zeta = 20(rad/s)^2$$
$$m_t = 25(N \cdot m)^2$$
$$\text{Load change state:} \qquad m_{tl} = 5 \times 10^4 (N \cdot m)^2$$
$$\text{steady state:} \qquad m_{tl} = 100(N \cdot m)^2$$

The MPC controller operates with a 50ms sampling period in the embedded system. The prediction horizon and control horizon are set to 6 and 2 steps, respectively. The different sampling periods for the MPC ($t_{s1} = 50$ms) and the Kalman filter ($t_{s2} = 10$ms) were chosen deliberately to achieve an optimal balance between computational feasibility and estimation/control performance. The MPC algorithm involves computationally intensive online optimization (solving a QP problem). A longer sampling period is necessary to provide sufficient time for the embedded processor to reliably compute the optimal control moves within each cycle, ensuring real-time implementation stability. The Kalman filter is a relatively simple second-order linear observer. Its low computational cost permits a much faster sampling rate. This is crucial for achieving the primary design goal of the estimator: to rapidly track transient load torque changes. A faster update rate allows for quicker detection of load steps and more timely adaptation of the gain-scheduling strategy, which directly enhances the transient performance of the overall control system.

An equilibrium point lookup table, predetermined from experimental data, enables the proposed gain scheduling strategy to achieve effective speed and AFR tracking control. Notably, the MPC controller configuration remains identical across all three Kalman filter implementations, with consistent weighting matrices: $q = \begin{bmatrix} 5 & 0 \\ 0 & 4 \end{bmatrix}$, $\quad r = \begin{bmatrix} 2 & 0 \\ 0 & 2 \end{bmatrix}$;

The relatively small values of qand rreflect the normalization of state variables to comparable orders of magnitude (p_2 and p_1 in kPa, ξ scaled by 1000). Experimental results are presented in Figures 5-8, focusing on the critical first-loading scenario where the generator set transitions from no-load to 30% of maximum load before unloading. The excess air coefficient λ, a normalized value defined as the ratio of the actual AFR to the stoichiometric AFR, is used in the experimental results.

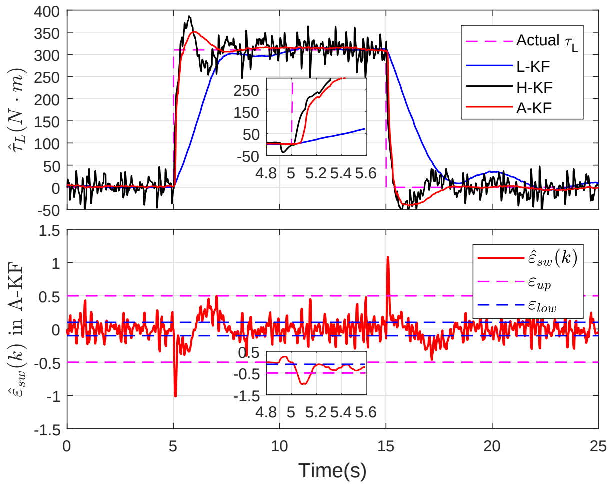

Figure 5. Estimated load torque comparison between three Kalman Filter

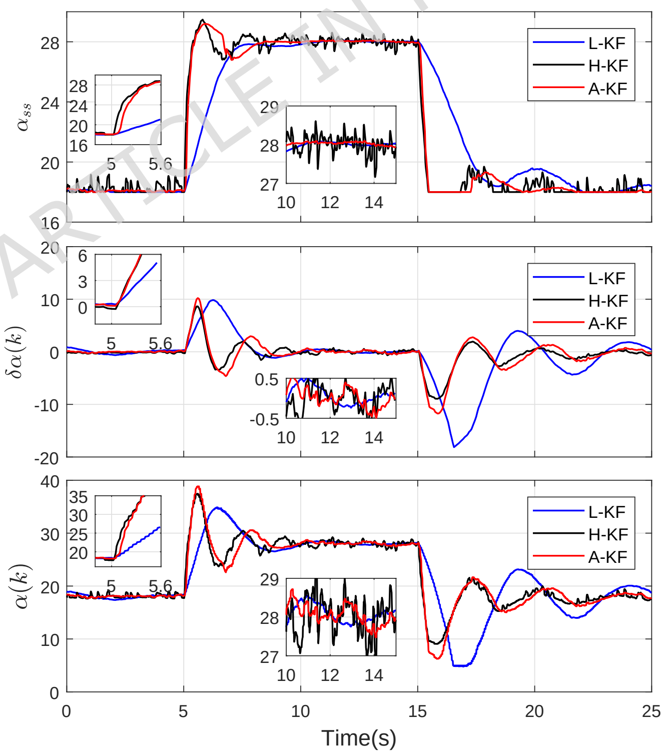

Figure 6. Mixture throttle opening comparison between three Kalman Filter

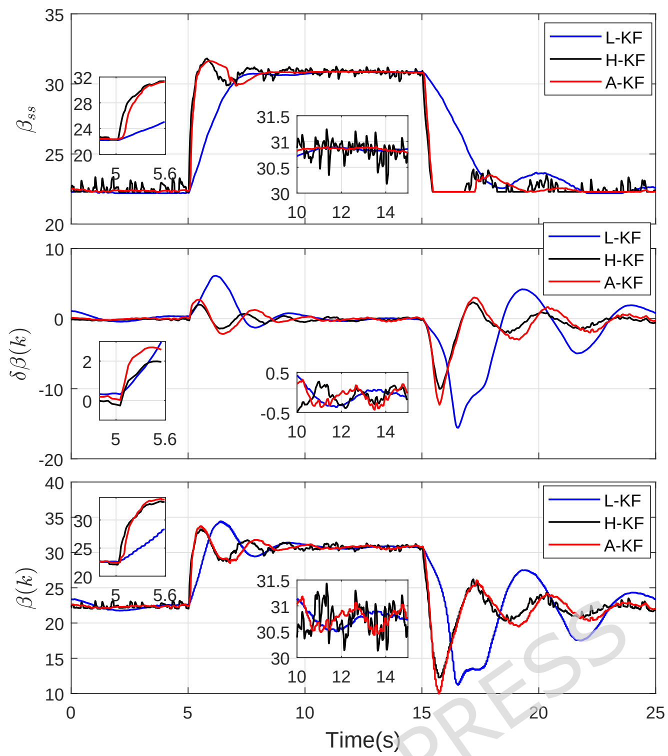

Figure 7. Fuel throttle opening comparison between three Kalman Filter

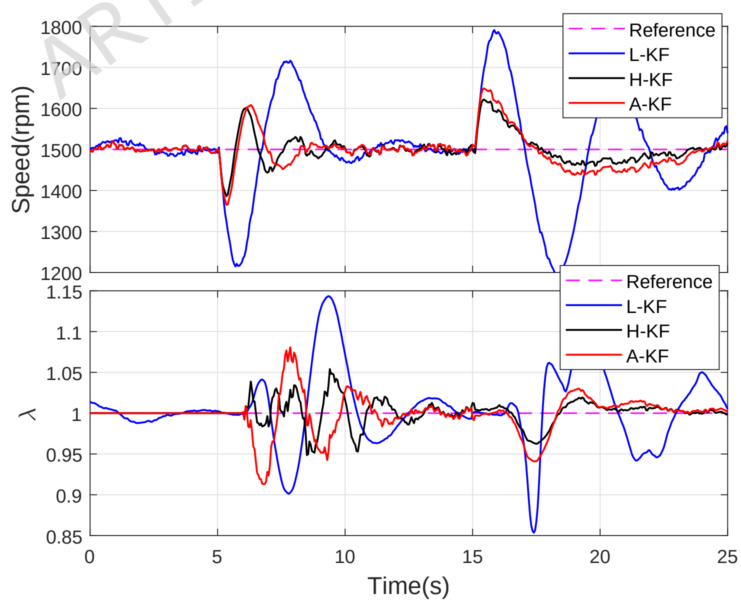

Figure 8. Output comparison of engine speed and AFR between three Kalman Filter

As shown in Figure 5, both H-KF and A-KF achieve rapid load torque tracking, converging within approximately 400ms, significantly outperforming L-KF. The H-KF's immediate convergence stems from its large, fixed m_{tl} value. The A-KF exhibits a slight delay relative to H-KF due to the detection mechanism's response time – approximately 60ms after the load change, $|\hat{\varepsilon}_{sw}(k)|$ exceeds the upper threshold ε_{up}, triggering the switch to high m_{tl} and accelerated convergence. When $|\hat{\varepsilon}_{sw}(k)|$ falls below the lower threshold ε_{low} around 400ms, m_{tl} reverts to its low value to ensure steady-state noise suppression. Both H-KF and A-KF provide sufficiently fast load estimates to enable rapid updates of the gain-scheduling matrix and equilibrium input u_{ss}.

Figures 6 and 7 demonstrate that α_{ss} and β_{ss} for H-KF and A-KF respond promptly after loading (at 5s), resulting in sharp increases in the final control inputs $\alpha(k)$ and $\beta(k)$. In contrast, L-KF's slow load estimation causes gradual changes in α_{ss} and β_{ss}, making the final inputs predominantly determined by the MPC outputs $\delta\alpha(k)$ and $\delta\beta(k)$. Consequently, as evident in Figure 8, L-KF exhibits substantial speed and AFR deviations following load changes, with speed excursions exceeding $\pm$200rpm and prolonged AFR settling times. H-KF and A-KF, however, limit speed fluctuations to approximately $\pm$150rpm through prompt input adjustments. (For reference, typical generator sets permit speed fluctuations around $\pm$10% of nominal speed.)

Regarding noise suppression, H-KF exhibits significant steady-state estimation noise due to its large m_{tl}, which propagates to u_{ss} and ultimately to the throttle commands, causing irregular fluctuations detrimental to precise throttle control. Both L-KF and A-KF demonstrate superior noise suppression. Analysis of the final control variables ($\alpha(k)$ and $\beta(k)$), reveals that noise primarily originates from the equilibrium inputs (α_{ss} and β_{ss}), while the MPC outputs ($\delta\alpha(k)$ and $\delta\beta(k)$) contribute minimal noise across all configurations.

	α_{ss}	$\delta\alpha$	α	β_{ss}	$\delta\beta$	β
H-KF	0.0647	0.0212	0.1238	0.0312	0.0112	0.0757
A-KF	0.0013	0.0189	0.0262	0.0003	0.0098	0.0145

Table 1. Comparison of steady-state variance of input variables in H-KF and A-KF (unit:$degree^2$)

Table 1 compares the steady-state variances of input variables for H-KF and A-KF during 10-15s (L-KF is excluded as its parameters match A-KF's steady-state values but with inferior dynamic performance). The variances of α_{ss}, α, β_{ss} and β are substantially larger in H-KF than in A-KF. Specifically, H-KF's α fluctuates within nearly $\pm$1 degree, while A-KF maintains fluctuations within $\pm$0.5 degree.

These results confirm the necessity of the adaptive A-KF strategy. While conventional Kalman filters can be tuned to balance tracking speed and noise rejection[27], static parameter tuning cannot simultaneously satisfy both requirements in this application. H-KF achieves acceptable transient performance but introduces excessive steady-state noise, whereas conservative (low-gain) tuning suppresses noise but fails to track rapid load disturbances. This trade-off is critical in practice since the filter output serves as the reference for throttle positioning – noisy references induce sustained throttle jitter, accelerate actuator wear, and may compromise system stability. The A-KF successfully reconciles these conflicting objectives by enhancing estimator responsiveness during transients while maintaining strong noise attenuation in steady state, thereby ensuring both performance and operational safety.

Comparative Experimental Evaluation

The proposed MPC framework with adaptive Kalman filter (AFK-MPC) was experimentally compared against two baseline methods: a conventional PI control strategy and the standard rate-based MPC without adaptation.

The conventional PI control method employs two decoupled PI controllers to regulate engine speed and AFR, respectively. For speed control, the PI controller directly computes the mixture throttle opening based on the error between the actual and target speed. The AFR control loop is more complex: to address the significant transport delay, a feedforward term based on intake manifold pressure (p_2) is incorporated, as suggested in[34]. In each control cycle, a base fuel throttle opening is determined from a p_2 lookup table. A PI controller then acts on the deviation between the measured AFR and its target, and its output is added to the base opening to yield the final fuel throttle command. This approach is referred to as Double-PI (D-PI) control. The final tuned parameters are: $k_{sp} = 1.3, k_{si} = 0.03$ for the speed PI controller, and $k_{ap} = -5, k_{ai} = -4$ for the AFR PI controller.

The rate-based MPC controller follows the design detailed in Section "MPC Controller Design", with its control block diagram identical to that shown in Fig.3(a). It utilizes the same parameter matrix as the AKF-MPC controller, which is derived from the A-KF configuration. As this approach employs a linear MPC formulation, it is referred to as LMPC throughout this paper.

Figures 9 - 11 present a comparative analysis of the load response performance among the AFK-MPC, LMPC, and PI controllers. The test sequence involved applying 30% of the maximum load at 10s, followed by an additional 200Nm at 30s,

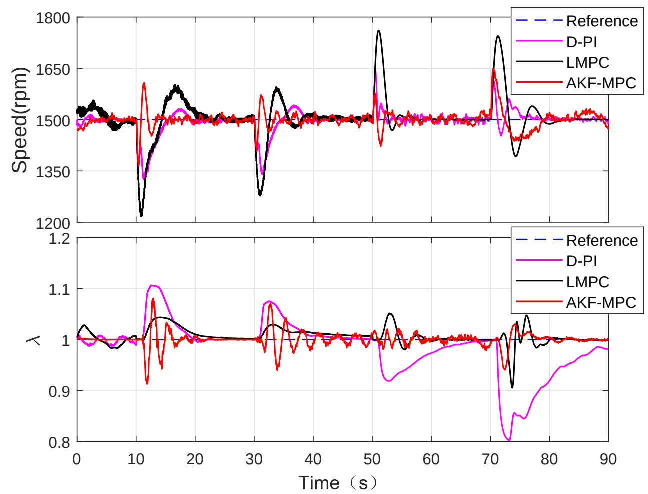

Figure 9. Comparison of engine speed and AFR responses for D-PI, LMPC, and AFK-MPC controllers.

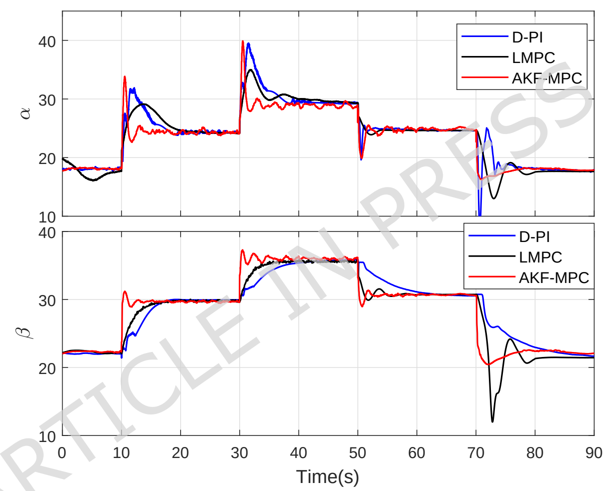

Figure 10. Comparison of control inputs for D-PI, LMPC, and AFK-MPC controllers

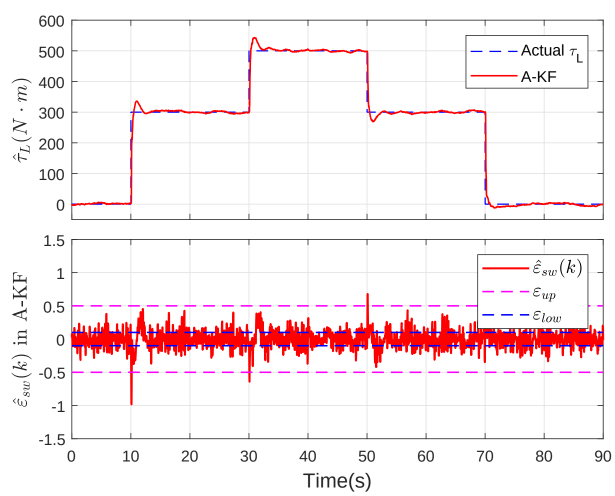

Figure 11. Comparison of the estimated load torque and its sliding-window average for the AFK-MPC.

Table 2. Quantitative comparison of controller performance during loading and unloading transients

Index	D-PI	LMPC	AFK-MPC
Average of speed settling time ($\pm 2\%$) [s]	6.875	7.943	5.146
Max deviation of speed [rpm]	-167 +155	-281 +269	-138 +149
Average of λ settling time ($\pm 2\%$) [s]	12.95	11.26	12.136
Max deviation of λ	-0.2 +0.11	-0.098 +0.052	-0.086 +0.084

with sequential unloading thereafter. Table 2 summarizes quantitative metrics for these loading and unloading processes.

In terms of speed control performance, the tuned D-PI controller achieves a level close to the power generation requirements. However, the LMPC, which relies solely on the rate-based MPC without load torque information, exhibits significantly degraded speed performance, similar to the L-KF results observed earlier. In contrast, the AFK-MPC, benefiting from the gain-scheduling parameter matrix and feedforward term u_{ss}, demonstrates markedly improved speed response, outperforming D-PI. The speed fluctuation of AFK-MPC remains within ± 150rpm, satisfying practical generation demands, and its settling time is significantly shorter than those of D-PI and LMPC.

Regarding AFR control, both LMPC and AFK-MPC show substantially smaller AFR fluctuations compared to D-PI. This improvement stems from the ability of MPC to coordinate multiple inputs in MIMO systems, whereas D-PI lacks inherent decoupling capability. Although the settling times for AFR are comparable across controllers, the overall AFR performance of LMPC and AFK-MPC is superior.

Based on these results, the AFK-MPC strategy delivers the best comprehensive performance: speed fluctuations remain within the required range, settling time is short, and AFR variations are minimal.

In practical applications, the adaptive load detection mechanism is typically triggered during transients. If not activated immediately upon loading, the controller's initial response is slower, leading to rapid speed deviation. This causes $|\hat{\varepsilon}_{sw}(k)|$to exceed the upper threshold ε_{up}, activating the adaptation. Only when the load is small enough that the rate-based MPC alone can quickly restore speed will the detection remain inactive, in such cases, speed deviation is negligible.

Conclusion

The main contribution of this paper lies in the proposal of a control method that integrates an adaptive Kalman estimator with a gain scheduling strategy, combined with rate-based model predictive control (MPC), which significantly enhances the system's anti-disturbance performance under unknown load variations. The paper elaborates on the design process of the MPC controller and the adaptive Kalman filter: by introducing an adaptive strategy and a load variation detection mechanism, the Kalman filter achieves rapid tracking of load torque changes under transient conditions while effectively suppressing estimation noise in steady-state operation, thereby balancing dynamic response speed and steady-state accuracy.

The proposed method exhibits strong engineering applicability. Since model linearization, discretization, and prediction model computations can be performed offline, the online computational burden of MPC is reduced to solving a QP problem, significantly lowering the computational load. Moreover, the Kalman filter features a simple structure with minimal online computational requirements, making it suitable for implementation in embedded systems. Experimental results demonstrate that the control framework effectively suppresses speed and AFR fluctuations caused by step load changes, shortens the settling time, and provides a feasible solution for improving the load adaptability of natural gas engines used in power generation.

References

1. Kou, C. *et al.* Collaborative optimization design of intake and combustion chamber structures for heavy-duty natural gas engines under knock limitation. *Energy* **316**, 134662, DOI: https://doi.org/10.1016/j.energy.2025.134662 (2025).

2. Tang, Y. *et al.* Challenges and opportunities of natural gas dual-fuel engines for marine applications. *Fuel* **400**, 135808, DOI: https://doi.org/10.1016/j.fuel.2025.135808 (2025).

3. Tayyeban, E. & Deymi-Dashtebayaz, M. Optimizing an expansion engine-based organic rankine cycle system for heat recovery from natural gas engines. *Energy Convers. Manag.* **343**, 120209, DOI: https://doi.org/10.1016/j.enconman.2025.120209 (2025).

4. Lino, P., Maione, B. & Amorese, C. Modelling and predictive control of a new injection system for compressed natural gas engines. *Control. Eng. Pract.* **16**, 1216–1230, DOI: https://doi.org/10.1016/j.conengprac.2008.01.008 (2008).

5. Thompson, J. S., Walton, S., Hassan, O., Rolland, S. A. & Sienz, J. The use of cfd and multi-objective optimisation techniques to customise an industrial pre-mixer. *Struct. Multidiscip. Optim.* **55**, 2339–2351, DOI: https://doi.org/10.1007/s00158-016-1643-7 (2017).

6. Gong, Q., Xu, J., Ye, J., Feng, H. & Shen, A. Nonlinear model predictive control for premixed turbocharged natural gas engine. *IEEE/ASME Transactions on Mechatronics* **27**, 3694–3705, DOI: 10.1109/TMECH.2021.3130910 (2022).

7. Keller, M. *et al.* Model predictive air path control for a two-stage turbocharged spark-ignition engine with low pressure exhaust gas recirculation. *Int. J. Engine Res.* **21**, 1835–1845, DOI: https://doi.org/10.1007/s38313-020-0295-6 (2020).

8. Koli, R. *et al.* Nonlinear model predictive control of dual loop - exhaust gas recirculation in a turbocharged spark ignited engine. In *2018 Annual American Control Conference (ACC)*, 2437–2442, DOI: 10.23919/ACC.2018.8430853 (2018).

9. Bergmann, D., Harder, K., Niemeyer, J. & Graichen, K. Nonlinear mpc of a heavy-duty diesel engine with learning gaussian process regression. *IEEE Transactions on Control. Syst. Technol.* **30**, 113–129, DOI: 10.1109/TCST.2021.3054650 (2022).

10. Di Cairano, S., Doering, J., Kolmanovsky, I. V. & Hrovat, D. Model predictive control of engine speed during vehicle deceleration. *IEEE Transactions on Control. Syst. Technol.* **22**, 2205–2217, DOI: 10.1109/TCST.2014.2309671 (2014).

11. Di Cairano, S., Yanakiev, D., Bemporad, A., Kolmanovsky, I. V. & Hrovat, D. Model predictive idle speed control: Design, analysis, and experimental evaluation. *IEEE Transactions on Control. Syst. Technol.* **20**, 84–97, DOI: 10.1109/TCST.2011.2112361 (2012).

12. Zhu, Q., Onori, S. & Prucka, R. An economic nonlinear model predictive control strategy for si engines: Model-based design and real-time experimental validation. *IEEE Transactions on Control. Syst. Technol.* **27**, 296–310, DOI: 10.1109/TCST.2017.2769660 (2019).

13. Zhou, J., Fiorentini, L., Canova, M. & Wang, Y. Coordinated performance optimization of a variable geometry compressor with model predictive control for a turbocharged diesel engine. *IEEE Transactions on Control. Syst. Technol.* **24**, 804–816, DOI: 10.1109/TCST.2015.2468085 (2016).

14. Hu, C., Wei, X. & Ren, Y. Passive fault-tolerant control based on weighted lpv tube-mpc for air-breathing hypersonic vehicles. *Int. J. Control. Autom. Syst.* **17**, 1957–1970, DOI: https://doi.org/10.1007/s12555-018-0594-8 (2019).

15. Santillo, M. & Karnik, A. Model predictive controller design for throttle and wastegate control of a turbocharged engine. In *2013 American Control Conference*, 2183–2188, DOI: 10.1109/ACC.2013.6580159 (2013).

16. Huang, M., Zaseck, K., Butts, K. & Kolmanovsky, I. Rate-based model predictive controller for diesel engine air path: Design and experimental evaluation. *IEEE Transactions on Control. Syst. Technol.* **24**, 1922–1935, DOI: 10.1109/TCST.2016.2529503 (2016).

17. Rigatos, G., Siano, P. & Ingenito, G. Controller design for agvs and kalman filter-based compensation of disturbance forces and torques. *Intell. Ind. Syst.* **2**, 197–216, DOI: 10.1109/CIVEMSA.2013.6617412 (2016).

18. Fu, J. *et al.* Research on Optimization of Diesel Engine Speed Control Based on UKF-Filtered Data and PSO Fuzzy PID Control. *Processes* **13**, 777, DOI: 10.3390/pr13030777 (2025).

19. Mercorelli, P. A hysteresis hybrid extended kalman filter as an observer for sensorless valve control in camless internal combustion engines. *IEEE Transactions on Ind. Appl.* **48**, 1940–1949, DOI: 10.1109/TIA.2012.2226193 (2012).

20. Pourbabaee, B., Meskin, N. & Khorasani, K. Sensor fault detection, isolation, and identification using multiple-model-based hybrid kalman filter for gas turbine engines. *IEEE Transactions on Control. Syst. Technol.* **24**, 1184–1200, DOI: 10.1109/TCST.2015.2480003 (2016).

21. Pavkovic, D., Deur, J. & Kolmanovsky, I. Adaptive kalman filter-based load torque compensator for improved si engine idle speed control. *IEEE Transactions on Control. Syst. Technol.* **17**, 98–110, DOI: 10.1109/TCST.2008.922556 (2009).

22. Yang, Q., Li, S. & Cao, Y. A strong tracking filtering approach for health estimation of marine gas turbine engine. *J. Mar. Sci. Appl.* **18**, 542–553, DOI: https://doi.org/10.1007/s11804-019-00103-8 (2019).

23. Zerdali, E. Strong tracking extended kalman filter based speed and load torque estimations of induction motor. In *2019 1st Global Power, Energy and Communication Conference (GPECOM)*, 216–221, DOI: 10.1109/GPECOM.2019.8778455 (2019).

24. Huang, M., Nakada, H., Polavarapu, S., Butts, K. & Kolmanovsky, I. Rate-based model predictive control of diesel engines. *IFAC Proc. Vol.* **46**, 177–182, DOI: https://doi.org/10.3182/20130904-4-JP-2042.00094 (2013). 7th IFAC Symposium on Advances in Automotive Control.

25. Ferreau, H. J., Kirches, C., Potschka, A., Bock, H. G. & Diehl, M. qpoases: a parametric active-set algorithm forquadratic programming. *Math. Program. Comput.* **6**, 327–363, DOI: https://doi.org/10.1007/s12532-014-0071-1 (2014).

26. Danijel Pavković, V. I., Joško Deur & Hrovat, D. Si engine load torque estimator based on adaptive kalman filter and its application to idle speed control. *SAE Transactions* **114**, 71–82, DOI: https://doi.org/10.4271/2005-01-0036 (2005).

27. Chui, C. K. & Chen, G. *Orthogonal Projection and Kalman Filter*, chap. 3, 33–49 (Springer International Publishing, Cham, 2017).

28. Wang, X. & Huang, Y. Convergence study in extended kalman filter-based training of recurrent neural networks. *IEEE Transactions on Neural Networks* **22**, 588–600, DOI: 10.1109/TNN.2011.2109737 (2011).

29. Gustafsson, F. *Change Detection Based on Sliding Windows*, chap. 6, 205–230 (John Wiley and Sons, Ltd, 2000).

30. Boutayeb, M., Rafaralahy, H. & Darouach, M. Convergence analysis of the extended kalman filter used as an observer for nonlinear deterministic discrete-time systems. *IEEE Transactions on Autom. Control.* **42**, 581–586, DOI: 10.1109/9.566674 (1997).

31. Yang, H., Xia, Y., Shi, P. & Fu, M. A novel delta operator kalman filter design and convergence analysis. *IEEE Transactions on Circuits Syst. I: Regul. Pap.* **58**, 2458–2468, DOI: 10.1109/TCSI.2011.2131330 (2011).

32. Rugh, W. J. & Shamma, J. S. Research on gain scheduling. *Automatica* **36**, 1401–1425, DOI: https://doi.org/10.1016/S0005-1098(00)00058-3 (2000).

33. Huang, M., Butts, K. & Kolmanovsky, I. A low complexity gain scheduling strategy for explicit model predictive control of a diesel air path. In *8th ASME Annual Dynamic Systems and Control Conference (DSCC 2015)*, 01–10, DOI: 10.1115/DSCC2015-9754 (ASME, 2016).

34. Su, H., Hao, G., Li, P. & Luo, X. Feed forward fuzzy pid controller for common-rail pressure control of diesel engine. In *2010 International Conference on Measuring Technology and Mechatronics Automation*, vol. 2, 264–267, DOI: 10.1109/ICMTMA.2010.600 (2010).

Acknowledgements

This work was supported by the National Natural Science Foundation of China (Grant No. 62403212).

Funding

This work was supported by the National Natural Science Foundation of China (Grant No. 62403212).

Author contributions statement

Wenyu Xiong conceived the study, designed the experiments, and wrote part of the manuscript. Qichangyi Gong conducted the experiments, analyzed the data and wrote part of the manuscript. Songtao Huang, Jie Ye, and Jinbang Xu performed data curation, validation, and provided critical feedback on the manuscript. All authors reviewed and approved the final manuscript.

Data availability statement

The datasets generated during and/or analysed during the current study are available from the corresponding author on reasonable request.

Additional information

The authors declare no competing interests.